Device Fabrication on Topological Insulators and probing Ferroelectricity

Shivam Mishra

A dissertation submitted for the partial fulfillment of BS-MS dual degree in Science

Department of Physical Sciences
Indian Institute of Science Education and Research,
Mohali

April 2019

Certificate of Examination

This is to certify that the dissertation titled "**Device Fabrication on Topological Insulators and probing Ferroelectricity** " submitted by Shivam Mishra (Reg. No. MS14188) for the partial fulfillment of BS-MS dual degree program of the institute, has been examined by the thesis committee duly appointed by the institute. The committee finds the work done by the candidate satisfactory by the institute and recommends that the report be accepted.

Dr. Yogesh Singh | Dr. Sanjeev Kumar | Dr. Goutam Sheet (Supervisor)

Declaration

The work presented in this dissertation has been carried out by me under guidance of Dr. Goutam Sheet at the Indian Institute of Science Education and Research, Mohali.

This work has not been submitted in part or in full for a degree, a diploma, or a fellowship to any other university or institute. Whenever contributions of others are involved, every effort is made to indicate this clearly, with due acknowledgement of collaborative research and discussions. This thesis is a bona-fide record of original work done by me and all sources listed within have detailed in the bibliography.

Shivam Mishra
(Candidate)

Dated: April 25, 2019

In my capacity as the supervisor of the candidate's project work, I certify that the above statements by the candidate are true to the best of my knowledge.

Dr. Goutam Sheet
(Supervisor)

Acknowledgements

Firstly, I would like to express my sincere gratitude to my advisor Dr. Goutam Sheetwhose constant guidance and encouragement has motivated me to carry out this project with new enthusiasm every day. The time and effort he gives towards ongoing projects in lab has motivated and inspired me to continue research in future.

I would also like to thank my thesis committee members for their valuable suggestions and feedback.

This work would not have been possible without the help and support of my labmates. I would like to thank *Aastha and Suman* for their help in optimizing the projection lithography system. I would also like to thank *Veerpal* for helping and collaborating with me in various experiments. Thanks are also due to *Lalit, Aastha and Rajeshwari Di* for guiding me in initial stages in the lab. I also thank *Shekhar, Anshu, Ritesh, Suman, Sandeep, Deepti, Monika, Soumyadeep and Soumya* who have helped me in many ways. Thanks to *Ranjana* for help in smooth functioning of the lab. All credits go to my lab mates for making SPIN lab a beautiful place to work in. I learned a lot from you all.

I am indebted to Neha and Ruchi from INST for providing photoresist and developer for projection lithography. I would also like to thank *Dr. RK Gopal* for providing BSTS crystals. I am indebted to Neha for providing STO samples.

I am grateful to my friends *Sanjay, Aj, Dharma, Pawan, Vasu and Vishal* for the fun and laughter I had with them in last five years.

Finally, I would thank my parents and sisters who are behind every good things that happen in my life.

List of Figures

1.1 Cyclotrons motion of electrons in bulk and conduction along the edge and quantized hall resistivity at low temperatures 4
1.2 Deformation of sphere to donut is a topological transition but cup and donut are topologically equivalent 5
1.3 E vs k dispersion relation of topological insulator showing linear dispersion surface states 6
1.4 Spin momentum locked helical transport in topological insulators . . . 7
1.5 Schematic of hall bar device over a topological insulator 9
1.6 Image of projection lithography system 11
1.7 The binary image of pattern transferred on resist 13
1.8 The binary image of pattern transferred on resist 14
1.9 SEM image of final device 15
1.10 zoomed SEM image of final device showing contacts over BSTS 15

2.1 Schematic of optical lever detection method 20
2.2 Laser spot after vertical deflection of cantilever 23
2.3 Oscillation amplitude near and above the sample 25

3.1 Schematic of PFM set up 28
3.2 Combination of AC and DC signal in triangular saw tooth form for PFM spectroscopy 29
3.3 Frequency vs oscillation amplitude showing the resonant frequency . . 30
3.4 Phase vs V_{dc} switching curve at temperature (a) 278K (b) 283K (c) 300K and (d) 323K 31
3.5 Temperature dependence of amplitude vs DC Bias (Butterfly loop) . . 32
3.6 Topographic image before and after PFM spectroscopy 33
3.7 Amplitude and phase images resembling the topographic image 33

Abbreviations

um	**m**icro **m**eter
pm	pico meter
laser	**l**ight **a**mplification by **s**timulated **e**mission of **r**adiation
PZT	Piezo electric actuator
AFM	Atomic force microscopy
SEM	Scanning electron microscope

Contents

Certificate of Examination iii

Declaration v

Acknowledgements vii

List of Figures ix

Abbreviations xi

Abstract xvii

I First Part 1

1 Electron Transport in Topological Insulator 3
1.1 Preliminary . . . 3
1.2 Electron Transport in Topological Insulators . . . 7
1.3 Device Fabrication . . . 8
1.3.1 Projection Lithography . . . 11
1.3.2 Gold Deposition . . . 12
1.3.3 Lift-off . . . 13
1.4 Results . . . 14

II Second Part 17

2 Atomic force microscopy 19
2.1 Introduction . . . 19
2.1.1 Atomic force microscopy . . . 20

2.1.2 Tip sample interaction 20
2.1.3 Components of AFM 21
2.1.3.1 Piezo Actuators and Scanners 21
2.1.3.2 Cantilever tip 22
2.1.3.3 Optical Lever Detection 22
2.1.3.4 Feedback mechanism 23
2.1.4 Operational Modes 24
2.1.4.1 Non-Contact mode 24
2.1.4.2 Contact mode 26

3 Local Ferroelectricity in Ge doped SnTe 27
3.1 Introduction 27
3.2 PFM set up 28
3.2.1 DART PFM 29
3.3 PFM Spectroscopy 29
3.4 Results 30
3.5 Conclusion 34

Bibliography 35

Dedicated to my parents and sisters

Abstract

This thesis consists of two parts. In the first part, we are trying to see the surface dominated electron transport in nanoflakes of a topological insulator. The Bi based material, was recently reported to show suppressed bulk conductivity. This gives us a platform to study surface dominated transport in this material.I have made a device over topological insulator material using a variant of photo lithography system. Optimal parameters are found for the whole process. A Hall bar device is fabricated over the material which was to be used for studying surface dominated electron transport in Topological Insulators.

In second part, Piezoresponse force microscopy is used to study local ferroelectric polarization in a thermoelectric material. The material was supposed to have a good thermoelectric performance induced via structural distortions in lattice. These distortions are supposed to bring ferroelectric instability in material. Here, we show that local ferroelectricity do exist in material in the absence of global ferroelectric ordering.

Part I

First Part

Chapter 1

Electron Transport in Topological Insulator

1.1 Preliminary

The progress in condensed matter physics is generally driven by development of new materials to sustain the improvements in current electronic devices. Materials are generally divided into three subcategories based on their electrical conduction properties namely 1) Metals which are conducting, 2) Semiconductors, which can be made conducting by doping or temperature and 3) Insulators which do not conduct electricity. This division is based on the gap between the conduction and valence band states in these materials. Recently, a new type of material was reported which behaved as insulators in the bulk but had conducting edge states. These materials are called Topological Insulators. They are called "topological" because the wavefunction describing their electronic states span a Hilbert space which has non trivial topology[1]

All the phases of matter are described by associated symmetries of the system. An order parameter emerges in every broken symmetry state or ordered phase of a system[2]. Ginzburg Landau theory had enjoyed immense success with the exception being the discovery of Integer quantum hall effect. The experiment was done to study the behaviour of electrons confined in two dimensions subjected to perpendicular magnetic field and in plane electric field. As compared to classical Hall effect which had linear or transverse conductivity as a function of applied magnetic field, the hall conductivity

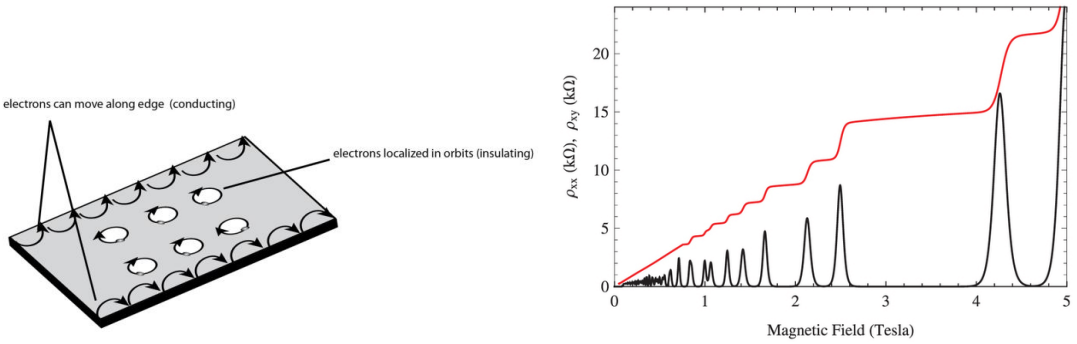

FIGURE 1.1: Cyclotrons motion of electrons in bulk and conduction along the edge and quantized hall resistivity at low temperatures
https://topocondmat.org/w3_pumpQHE/QHEedgestates

in QHE has step like plateaus at some values of magnetic field[3]. The measured Hall conductance was found to be quantized in units of e^2/h . The situation is described in figure 1. Note that the value of Hall resistance can be measuresd to a high degree of accuracy of 10^{-9} and can be used as unit of resistance or conductance[4]. In the regime of quantization, the longitudinal resistance vanishes to zero. The new, emerged state could not be described by previous known symmetry breaking rules. The state does not break any symmetry other than time reversal symmetry due to the presence of magnetic field. This quantized Hall resistance showed plateau like features. The Hall resistance is immune to impurities and other defects on the samples. So the Quantum Hall insulator is a bulk insulator unless the chemical potential is aligned with one of the plateaus.

One of the important understanding developed in the process to understand the quantized hall conductance, was the topological significance of the plateaus. It can be explained in terms of topological invariant called the "Chern number".[2]

Topology, a branch of mathematics related to the classification of geometrical objects which can be smoothly deformed in to each other without making any cut (topological phase transition). The most common example of topology is "Cup and donut". We cannot convert a cup into a donut without making any cuts or holes in it. In other words, cup and donut are topologically distinct. Geometry and topology are, in this way, linked by famous Gauss Bonnet theorem. The following mathematical condition

can be understood in the context of physics of QHE. The band insulating state or any metallic state cannot be deformed in to each other unless the connecting line in the QHS is broken or cut. Therefore these two band structures are topologically distinct and this distinction lies in the bulk band structure. Therefore, topologically equivalent objects have certain topological order parameter known as topological invariants/quantum number and this number does not change as one object is deformed in to another.[**?**]

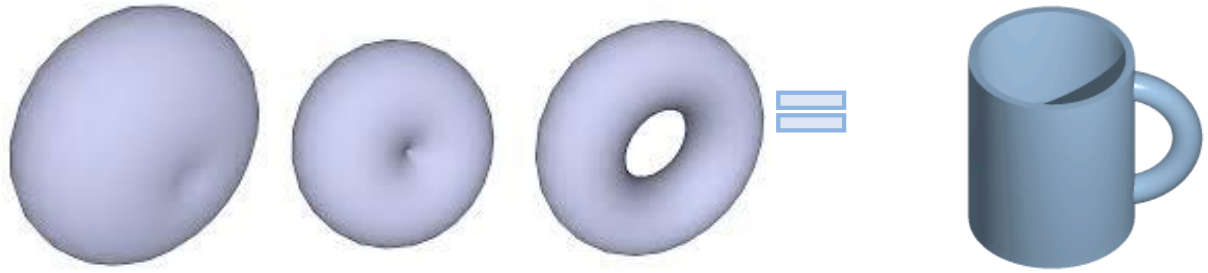

FIGURE 1.2: Deformation of sphere to donut is a topological transition but cup and donut are topologically equivalent

The integer quantum hall phase is protected to being deformed into phase with a different topology. Such a change is only possible if a phase transition occurs and the gap closes. Later it was realized that these topological order can also be realized in three dimensional materials without any presence of external magnetic field. The role of external magnetic field is played by spin orbit coupling in these materials. In three dimensional topological insulators, the bulk is insulating but the surface has metallic surface states.

The realization of quantized edge states in zero magnetic field, was first hypothetically predicted by Kane and Mele[5]. They considered a model of graphene and incorporated spin orbit coupling in the model. In graphene, the band structure has two linearly dispersing cones at different points in Brillouin zone[6]. The physics in these cones are described by employing the Dirac equation with rest mass set to be

zero; the dispersion being called the Dirac cone and the electrons behave as *massless Dirac fermions*.Unlike quantum Hall effect the time reversal symmetry (TRS) in this model was preserved due to absence of external magnetic field. Therefore the search for a material system with TRS preserved (with no external magnetic field) led to the discovery of the two dimensional and three dimensional topological insulators.
One such idea was proposed by S.C. Zhang group. They theoretically predicted that the sandwiched quantum wells heterostructures of HgCdTe exceeding a critical thickness $Tc = 6.3$ nm could be an ideal system to realize quantum hall like edge states with no external magnetic field applied[7].

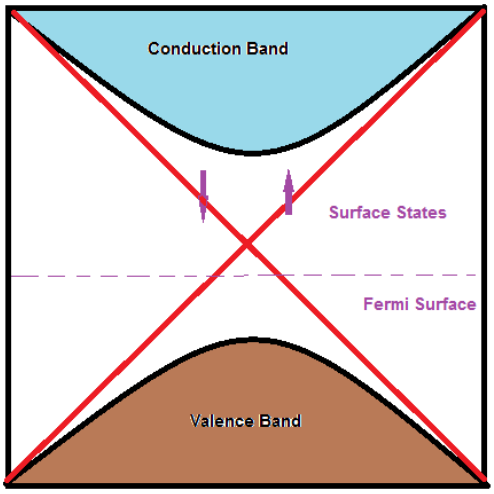

FIGURE 1.3: E vs k dispersion relation of topological insulator showing linear dispersion surface states

Topological insulators, with their nontrivial topology, are protected under time reversal symmetry. The gapless edge or surface states in these system present Dirac dispersion and thus provide a platform to study the relativistic physics of *Dirac fermions*. Further, the spin degeneracy is lifted for Dirac fermions residing in gapless surface states. Their spin is locked to the momentum, a state called "*helical spin polarization*". This is known as bulk boundary correspondence where bulk electronic structure is responsible for the appearance of the unusual surface states like in Quantum Hall effect. This quantized helicity is responsible for the immunity of these states towards impurities and disorder present in the realistic samples. It provides an opportunity to realize the Majorana fermions, which are considered as potential candidates for physical realization of quantum computer[8].

1.2 Electron Transport in Topological Insulators

Strong spin orbit coupling would be the primary requirement for a material to be a good topological insulator. After the experimental realization of Quantum spin Hall effect in HgCdTe based quantum wells, the search for 3D topological insulator began. It was again predicted by SC Zhang led group that Bi based materials like $Bi_2Se_3, Bi_2Te_3 and Sb_2Te_3$ are good candidates for realization of 3D topological insulators[9]. The first experimental confirmation came from the group of MZ Hassan at Princeton[10]. The surface band structure mapped in their experiment resolved the linear dispersed topological bands. With the experimental realization of 3D topological insulators and their peculiar characteristic of a helical spin current motivated the researchers to study electron transport solely through the surface states of these materials.

Until recently, surface dominated electron transport could not be found in any of the

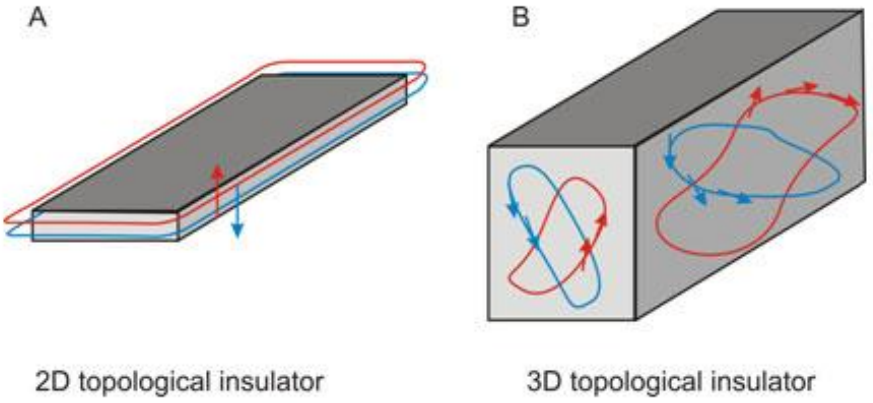

FIGURE 1.4: Spin momentum locked helical transport in topological insulators

topological insulators. Experimental techniques probing these surface states such as angle resolved photoemission spectroscopy, scanning tunneling microscopy and spectroscopy as well as electrical measurement techniques have unequivocally captured

signature of surface Dirac fermions till now. The nontrivial topology of the bulk band structure and spin momentum locking due to high spin-orbit interaction in these materials could revolutionize conventional electronic devices. Quantum Hall effect in three dimensions TI has recently been observed in these materials after a long period of 25 years after its two dimensional counterpart had been discovered.
To observe a clear signature of Dirac fermions and associated exotic phenomena one needs a highly insulating bulk with zero or negligible contribution to conductivity from bulk electrons and a super metallic surface conduction. But it was not possible with the second generation bismuth or antimony based TIs such as $Bi_2Se_3(BS), Bi_2Te_3(BT) and Sb_2Te_3$ (ST). These TIs were found to be heavily doped owing to the antisite defects and Se vacancies, resulting in them being a poor insulator in the bulk. Compensation doping in the bulk and application of gate voltage to locate the Fermi level in the bulk band gap have been used as a remedy to get rid of the afore mentioned problems with BS and BT. In 2016, a group from NTU Singapore, reported the synthesis of a Bi based material $Bi_{1.5}Sb_{0.5}Te_{1.8}Se_{1.2}$, shortly called BSTS, and observed surface dominated transport in nanoflake device of this material[11][12]. An insulating bulk is ensured by the location of the Fermi level in the bulk band gap. An ideal TI must have isolated Dirac cone, lesser hexagonal warping (lesser deformed Dirac cone), better spin texture and minimal contribution to bulk conduction which results in super metallic surface Dirac states. I have also tried to fabricate a hall bar device over nanoflakes of these material to study electron transport of these materials. The purpose is to make a dual gated device so that we can independently tune the chemical potential of top and bottom surface of topological insulator. By tuning the Dirac cone in the middle of band gap, we should see surface dominant transport in material.

1.3 Device Fabrication

To study electron transport in any material we need to make conducting metallic contacts over it. While this is easily possible in crystals of normal size, it becomes a bit tricky when the size of the material goes down. Here we are trying to fabricate Hall bar shaped device over micrometer sized flake which has thickness in nanometers. Schematic of Hall bar device is shown in figure. It consists of six electrodes over the sample. The outer two are used to supply bias and any other two are for measuring the

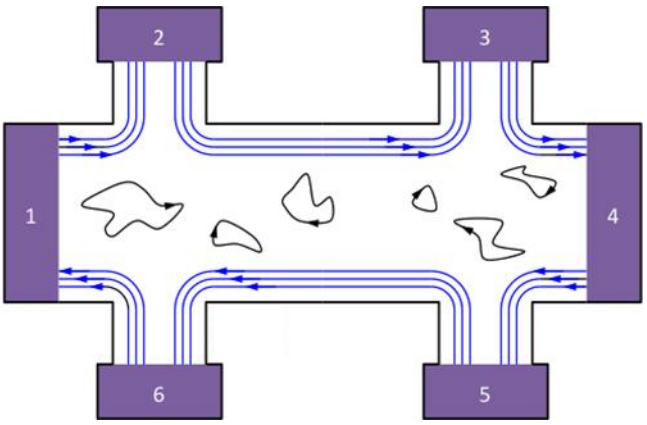

FIGURE 1.5: Schematic of hall bar device over a topological insulator

Transport in Semiconductor Mesoscopic Devices,CHAPTER 6, The quantum Hall effect,David K Ferry

response or current. The rest two electrodes are meant for gating and other external bias.

BSTS is an easily cleavable crystalline material. This means that it very easy to slice off thin flakes of this material from bulk crystals. We required a nanometer thickness flake of BSTS for our measurement. For this we need to cleave the bulk crystals. This was done using the standard scotch tape based method[13]. In this method we take a piece of the crystal and press it against a scotch tape gently. Another piece of scotch tape is pressed on the other side of material and is gently removed. This will decrease the thickness of the crystal. This process is repeated again, this time, on the same scotch tape but at a different position. The crytal is evenly spread over an area of the tape until the transparency of the tape region vanishes. This is a good indicator of good cleavability.

We need a substrate over which the sample will be transferred and the device made

over it. The choice of substrate plays an important role in transport measurement experiment. The preferred substrate should be insulating in character and inert to most elements. Moreover, it should have good planar surface and can be easily cleaned. The most preferred substrate is doped Si/SiO_2 wafer. The wafer consist of 0.5 mm thickness of Si. Since Si is easily oxidisable, a thin film of SiO_2 is always present on top of Si. Silicon is semiconductor but a doped silicon would have some conductivity. Si/SiO_2, on the other hand, is insulating and thus provides us a protective shield. The thickness of Si/SiO_2 over Si matters as current can tunnel through the small barriers (thickness of Si/SiO_2) and thus a direct connection between the two contacts will be established bypassing the sample. So generally, a substrate of Si with artificially grown Si/SiO_2 thickness of 300 nm is used.

The substrate is thoroughly cleaned by sonicating the wafers in acetone for 5 min and then washing them with Iso[ropyl alcohol. They are then blow dried using nitrogen blower. Now, to transfer the sample over the substrate, we just press the scotch tape over the material. The cleaving works on the principle of adhesion. When we press the sample over Si/SiO_2, the adhesion force between SiO_2 and BSTS exceeds that between intralayer attraction force in BSTS. Some layers of already cleaved BSTS sticks to the substrate. Using Atomic force microscopy, we measure the thickness of the flakes and found that the thickness ranged from 6 - 60 nm. To identify the flake with minimum thickness, we use an optical microscope. In optical microscope, flakes of different thickness will show different colour. The flake with very small thickness will be of nearly of same contrast as the surface of the substrate. This is the standard technique used to identify 2D materials. Moreover, we can also use Raman spectroscopy to measure the thickness or number of layers of the material.

We used projection lithography based technique to make contacts over the sample. This would be described in detail in next section. Standard lithographic techniques involve a photo or electron resist coating over a sample, which is then exposed in areas where you want the photoresist to be removed or hardened depending on the type of resist.

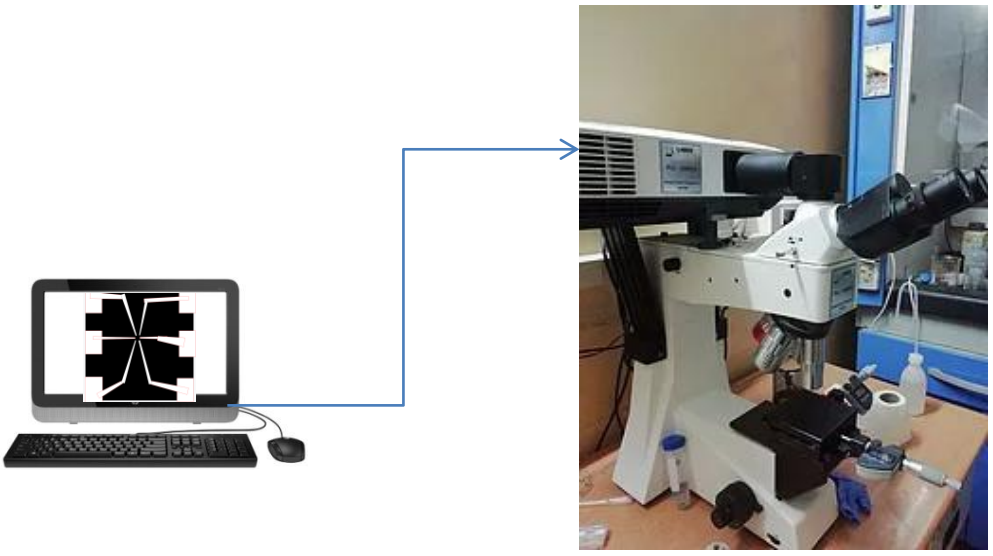

FIGURE 1.6: Image of projection lithography system

1.3.1 Projection Lithography

Standard photolithography techniques involve wafers coated with photoresist exposed to light in certain areas. A mask is placed in the area of the flake which is according to the shape of contacts to be made. Fabrication of these masks require electron lithography and pose many restriction to the type of device that can be fabricated. A new version of projection lithography which does not require any mask is developed using a projector and a optical microscope. The projector is connected to a computer which projects a black and white binary image through the microscope. The combination of lens inside the optical microscope condenses the beam of patterned light to small area of sample. A photograph of the system is attached in figure above.

With the magnification lens ranging from 10x to 100x, we can expose a maximumm area of 1mm to 100 micrometer. Since the magnification will also increase the resolution, there is always a thoroughput between resolution and maximum expose area. With increase in magnification, the scattering also increases which limits the resolution. The resolution that we were able to achieve was 2 micrometer but we could only expose 200 micrometer of the area. This was one of the problems which I faced during

this process. Also multiple exposure led to huge internal scattering and lithography was not successful.
Lithography begins by coating the resist on silicon wafer containing the flake. A drop of resist is placed over wafer and then it is spin coated at 5000 RPM for 30 seconds. The RPM determines the thickness of the coating over the sample. This is one of the key parameters which needs to be optimized according to needs. The coated wafer is then pre baked for few minutes to harden out the resist. The amount of prebake time and bake temperature is the second parameter that needs to be optimized. This in turn impacts the exposure time and dosage that is needed to loosen out the resist.

Now, the wafer is placed under the microscope. The patterned light is projected with a different wavelength so as to not expose the sample at first. The pattern is then adjusted over the flake and then the exposure is turned on. The patterned hall bar device is shown in figure. The exposure time is varied for different prebaking temperature. For prebaking temperature of 80^0C for 4 minutes, the optimized exposure time was found to be 8 seconds. After exposure the wafer is again baked for a minute before developing the resist. Developing the resist, is just removing the exposed resist with a reactant. The bonds become weak when resist is exposed to light. The developer solution then finds it easy to remove the resist from the exposed part. If the wafer is overdeveloped then it can dissolve the less exposed area of wafer where the light might have scattered to. So optimizing the developer time is of key importance. After developing, we see that the resist is removed from the exposed part.

1.3.2 Gold Deposition

To make metallic contacts over the sample, a thin layer of gold is deposited over the wafer using physical vapor deposition technique. Physical vapor deposition is a technique for material deposition for elements of boiling point below boiling point of tungsten. This is done by supplying large voltages through tungsten boats over which the elements are placed. The metals evaporate and get deposited over the wafers at room temperature placed directly above the boats. The thickness of the deposition is controlled by the amount of time the wafer is exposed to gold. The whole process is done in chambers with pressure of order of 10^{-6} mbar.

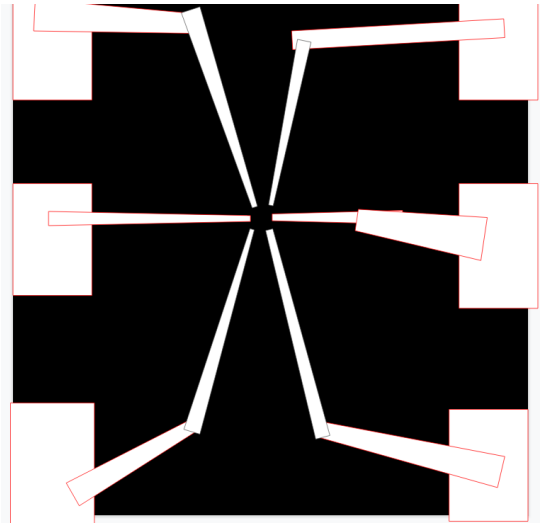

FIGURE 1.7: The binary image of pattern transferred on resist

Gold has a bad adhesion to the surface of Silicon wafer so first we deposit a thin layer of titanium and then gold is deposited over it. We deposit 100 nm of titanium and 400 nm of gold over the wafer. The wafer is now covered with gold and we need the contacts just in Hall bar shape. So we have to remove the deposited metals from other areas.

1.3.3 Lift-off

This is the process of removing the gold from unwanted areas of wafer. Note that photoresist is still beneath the metal layer in the unexposed areas of wafer. The metals are in contact with the wafer only in the areas where resist is removed. So, if we dissolve the photoresist, the gold above it will also be removed. This process is called lift off. This is done by dipping the wafer in acetone. This is most crucial part as gold should be removed from the areas just above the flake to ensure no external connections are there between any two contacts. This is final step of device fabrication.

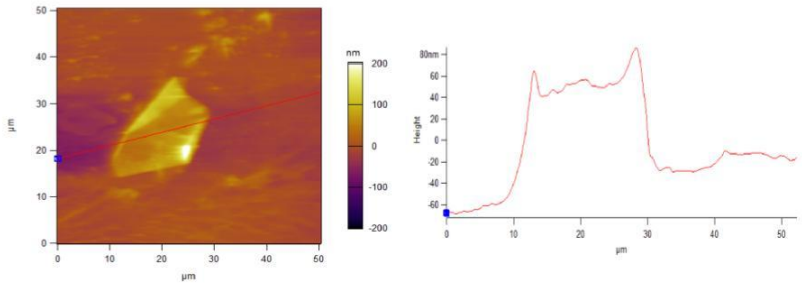

FIGURE 1.8: The binary image of pattern transferred on resist

1.4 Results

Thin flakes of BSTS were exfoliated using scotch tape based technique. The typical thickness of the flakes was found to be between 6 -60 nm. Topographic image of a flake is attached in the figure below. Width of flakes ranged from 2- 20 μm.

I was successful in optimizing the parameters of the projection lithography and then used it fabricate hall bar devices. The final hall bar device is shown in figure. I was not able to bond external wires to the big pads of gold contacts via wire bonding machine because the size of big goldpad was very small than that of the needle of the provided wire bonder. The average of big pads was just about 50 μm while the typical size needed for the wire bonding machine was 150-200 μm. Note that the size of the pads is controlled by the maximum area that can be exposed at a time which in turn is controlled by the resolution one needs. Moreover, multiple exposures method did not work as scattering was very large. The parameters were uncontrollable as the projector has a fixed dosage. The only parameter we could vary was exposure time. Proper resolution for a fixed exposure area could not be achieved. For a flake of size, $15x15\mu m$, the typical resolution needed is $2\mu m$. A SEM image of final device is shown in figure below. Due to unavailabilty of electron beam lithography, I could not continue with the project. So, I had to move on with other projects.

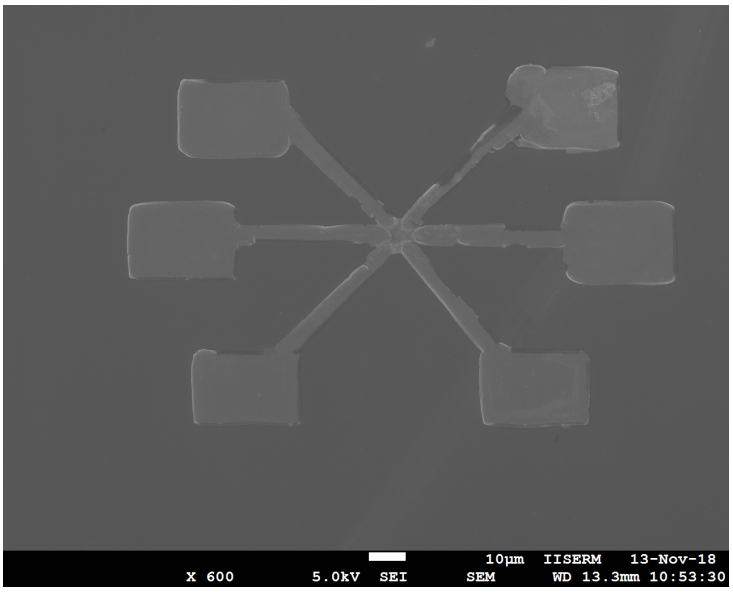

FIGURE 1.9: SEM image of final device

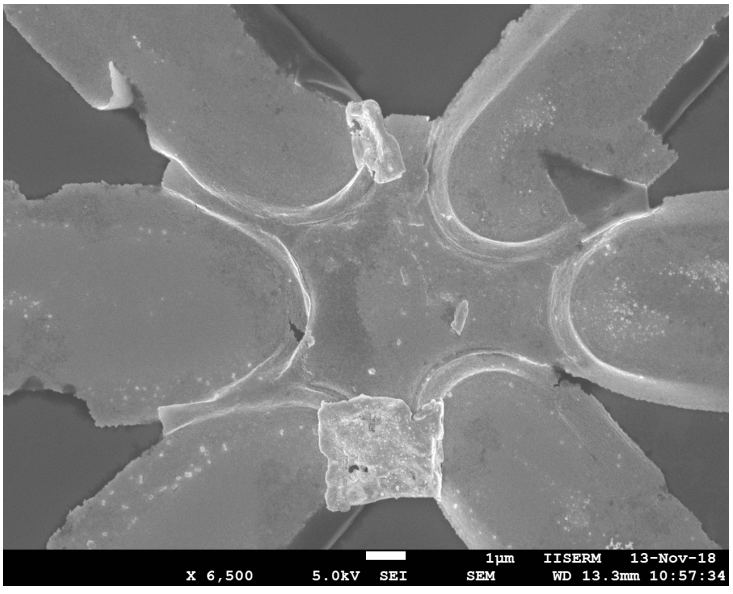

FIGURE 1.10: zoomed SEM image of final device showing contacts over BSTS

Part II

Second Part

Chapter 2

Atomic force microscopy

2.1 Introduction

Atomic force microscopy is a novel technique used to image and manipulate the surface topography of a material at small scale. These tools belong to the family of Scanning probe microscopy tools. Scanning probe microscopy (SPM) has emerged as a powerful tool for high resolution characterization of virtually all types of materials, including metals, semiconductors, dielectrics, polymers and biomolecules. SPM has also opened new venues in nanoscale domain patterning for such applications as high-density data storage.[14]

We use scanning probe microscopy in a number of different ways, depending on the information we are trying to gather from a sample. The two primary modes are contact mode and tapping mode. In contact mode, the force between the tip and the surface is kept constant. This allows a scientist to quickly image a surface. In tapping mode, the cantilever oscillates, just brushing the surface at its maximum deflection point. Tapping mode is especially useful when we are imaging a rough surface. [15]

A sharp tip moves back and forth over the sample to scan the surface. The tip is in close proximity to the sample and the interaction between the tip and sample give us information about the properties of sample like topography, polarization, conductivity and magnetic properties.[15] The interaction between tip and sample range from Van Der Waals force, Coulomb interaction to magnetic force.

2.1.1 Atomic force microscopy

The most common kind of scanning probe microscopy tool is Atomic force microscopy. Atomic force microscopy is a novel technique for high resolution imaging and spectroscopy. AFM consist of a nanoscale size tip mounted over a cantilever. The cantilever senses the interaction force between the tip and sample and depending on the interaction forces, the cantilever deflects from the original position. The deflection of the cantilever can be tracked via various methods. The most common method is optical lever method. In this method, a laser is directed onto the surface of the cantilever. Reflective coating on the cantilever reflects it back to a photodiode. The signal from the photo diode is read by lock in amplifier and the difference between the response signal and the original signal is minimized using a feedback loop.[16]

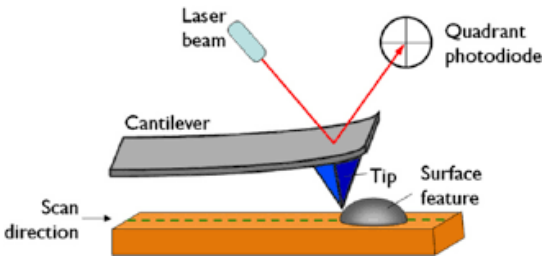

FIGURE 2.1: Schematic of optical lever detection method

The control signal from the lock in amplifier is used to estimate the properties of sample like topography, conductivity map etc.

2.1.2 Tip sample interaction

The interactive forces felt by the AFM tip are a combination of chemical interaction, electrostatic forces, magnetic forces, Van der Waals forces etc. The Van der Waals

forces can be approximated by Lennard-Jones potential. With this potential, one can estimate the interaction force between tip and the sample.

$$U(r) = 4\epsilon\left[-\frac{\sigma^7}{r^7} + \frac{\sigma^{13}}{r^{13}}\right] \tag{2.1}$$

where is an interaction parameter, r is the distance between the tip and the sample, and ϵ is a constant which depends on the geometry and material of the tip and the sample. The first term is the Van der Waals term and it characterizes the attractive force between tip and sample. The contribution of this term is significant when tip - sample distance is less than 10 nm.[16] However, at a separation smaller than 1 A^0, the overlap of electron clouds and ionic interaction causes strong repulsion between atoms of cantilever and sample surface. This repulsive interaction is captured in the second term of Lennard-Jones model. The forces between the tip of the cantilever and the sample are in the range of 10^7 10^{12} N. In order to produce a deflection significant enough to be detectable, micro-cantilevers with spring constant k less than .001 N/m are used. Further, to measure such a small force precisely it is necessary for the cantilever probe to be insensitive to the surrounding vibrations. The noise from the sources such as building vibrations has a power spectral density significant in the frequency range of 0-2 kHz. Hence, cantilevers with natural frequency more than 2 kHz are used and have dimensions around 100 x 10 x 2 um.[17]

2.1.3 Components of AFM

2.1.3.1 Piezo Actuators and Scanners

Piezoelectric effect is the property of certain materials to have mechanical deformations in response to an electric voltage. This property of piezo-electricity is exploited for the precise movement of tip at nanoscale. Piezos in AFMs are widely used for scanning. The piezo moves in a specific direction (expands or contracts) depending upon the voltage applied (positive or negative). The x-y motion of the sample is controlled by the piezos in the scanner and the z-motion of the tip is controlled by the piezo stack above the cantilever. The range of scanning area in AFMs is limited to few tens of microns. This is due to the nonlinear and hysteretic behavior of displacement of piezo with applied voltage. At high voltages problems like hysteresis and piezo

creeps become severe. Thus the accuracy of the displacement of the piezos is limited to few microns. The vertical (Z) motion of the tip is controlled by a piezo stack in the cantilever assembly.

2.1.3.2 Cantilever tip

The tip is the main working part of the AFM which actually interacts with the sample. It is a sharp micro-fabricated tip mounted at one end of an elastic cantilever.It is typically made up of Silicon or Silicon Nitride with a coating depending upon the choice of experiment. The radius of curvature of the tips apex is of the order of 5 50nm which limits the lateral resolution. The interactive force F between the tip and sample can given by Hooks Law.

$$F = k\Delta x \tag{2.2}$$

where k is elastic constant and the interactions between tip and sample are measured by the displacement of the cantilever Δ x.

2.1.3.3 Optical Lever Detection

Optical techniques are used to measure the motion of the cantilever as it interacts with the sample and is effected by various kinds of forces. A laser of wavelength 860nm is collimated and is focused on the tip using a lens. The beam reflects from the tip and is recollimated using a lens which is then reflected by a mirror reaching a segmented photo-diode. The bending of the cantilever can be detected optically as the laser spot moves up and down on the photo-diode itself. The angle of deflection is determined by position of photodiode. A small change in the angle leads to an amplified movement of laser spot on the photo-diode. Thus, photo-diode does not needs nanoscale precision to detect the motion of the

cantilever. The measurement of the cantilevers displacement has to be accurate in order to achieve atomic resolution. The cantilever may be deflected vertically or laterally which is detected optically using a segmented photo-diode having four quadrants as shown in Figure. The laser spot after reflecting from the tip falls on this segmented photo-diode. A voltage is generated for each quadrant depending on the

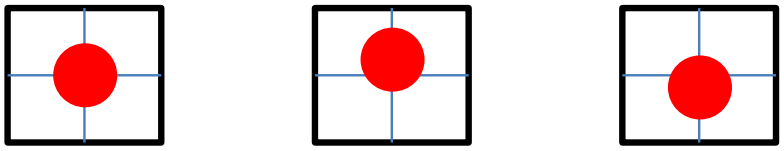

FIGURE 2.2: Laser spot after vertical deflection of cantilever

amount of the light falling on the corresponding segment. The vertical deflection is defined as the difference between the voltage generated in upper two and lower two quadrants whereas the lateral deflection is the difference between voltages generated in left and right quadrants. Figure shows the possible position of the laser spot on the photo-diode.

2.1.3.4 Feedback mechanism

An atomic force microscope can operate in many ways such as contact mode, where tip is directly in contact with the sample or tapping mode where tip grazes the sample in oscillatory manner. The details of the operational modes are discussed in the next section. In each of these modes, we have to set a setpoint parameter which will then be tracked and maintained at all the points. For instance, in contact mode, the feedback parameter is a deflection of the cantilever while in AC mode the oscillation amplitude of the cantilever serves as a feedback parameter. To track and maintain the setpoint such as deflection and oscillation amplitude, we change the value of z piezo according to our needs. This changes the distance betwen tip and sample. Thus, the movement of the z-piezo directly gives the height information. The feedback loop is implemented using the proportional-integral-derivative (PID) control, where integral gain plays the most crucial role in optimization of the feedback. If the gain is set too low, the PID loop will not be able to keep track of setpoint on the other hand if the gain is too high, noise signal will amplify strongly. The efficacy of feedback loop also depends on the scan rate. For a fast scan speed, PID loop will not have sufficient time to

react and adjust the feedback parameter to maintain the setpoint, and consequently, the topography calculated from z piezo movement will be inaccurate at slopes and near edges. However, for a very slow scan rate, there is no problem with the feedback but it increases the acquisition time which might make the measurement sensitive to thermal drift in the scan piezo.

2.1.4 Operational Modes

2.1.4.1 Non-Contact mode

The non-contact mode uses amplitude of oscillation of the cantilever as a feedback parameter. The shake piezo on the cantilever drives the cantilever at its resonant frequency with certain amplitude. The dynamic motion of a cantilever can be mimicked by a mechanically driven damped oscillator. The cantilever is driven by piezo with an external periodic force .

$$F_{drive} = kA_{drive}cos(\omega t) \tag{2.3}$$

The simple harmonic oscillator can thus be described by a second order differential equation.

$$m\frac{d^2z}{dt^2} = F_{drive} - b\frac{dz}{dt} - kz \tag{2.4}$$

where m is cantilevers mass, b is damping coefficient and z is vertical displacement of the cantilever. On solving,

$$A = \frac{A_{drive}\omega_o^2}{({\omega_c}^2 - \omega^2)^2 + \frac{\omega\omega_0}{Q^2}} \tag{2.5}$$

where is the instantaneous frequency, is the resonant frequency of the cantilever and Q is the quality factor which describes energy losses in a system. At resonance ($\omega = \omega^0$), the cantilever naturally oscillates with a greater amplitude as compared to any other frequency. As the distance between the cantilever and the sample is reduced, the amplitude of oscillation of the cantilever is damped due to inter-atomic forces between the tip and the sample.

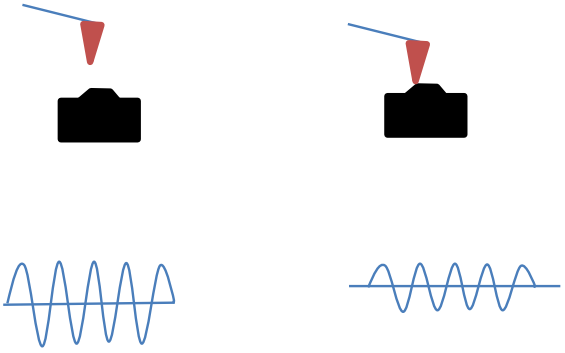

FIGURE 2.3: Oscillation amplitude near and above the sample

In order to implement AC mode, the cantilever is mechanically oscillated by a small piezoelectric actuator located near the cantilever chip, and the optical detector (segmented photodiode) senses the oscillatory motion of the cantilever from the corresponding oscillation in the laser spot. The acquisition of oscillating voltage signal generated at the photodiode is acquired using 5 MHz ADC which is then routed to a lock-in amplifier which retrieves the amplitude and phase with respect to drive signal. When the cantilever is away from the sample, it is tuned at its first resonance by mechanically vibrating it over a range of frequency using the piezo and noticing the amplitude response of the cantilever.

In order to implement AC mode, the cantilever is mechanically oscillated by a small piezoelectric actuator located near the cantilever chip, and the optical detector (segmented photodiode) senses the oscillatory motion of the cantilever from the corresponding oscillation in the laser spot. The acquisition of oscillating voltage signal generated at the photodiode is acquired using 5 MHz ADC which is then routed to a lock-in amplifier which retrieves the amplitude and phase with respect to drive signal. When the cantilever is away from the sample, it is tuned at its first resonance by mechanically vibrating it over a range of frequency using the piezo and noticing the amplitude response of the cantilever.

Once intrinsic fundamental frequency (f_0) of the cantilever is found it is driven near this frequency for rest of the experiment. At this point, driving frequency (fdrive) and cantilevers resonance frequency (f_0)are almost same and there is no phase difference between them. However, as the vibrating cantilever is approached near the sample and it begins to experience the attractive force, the effective resonant frequency (f_{eff}

) will decrease due to the force gradient as discussed earlier. The cantilever is now being driven at a frequency higher than its new resonance frequency (f_{eff}). From the graph, it can be seen that the amplitude change (A) at $f_{drive}(= f_0)$ very large even for a small change in intrinsic frequency.

2.1.4.2 Contact mode

In contact mode, the tip is dragged across the surface while raster scanning the sample. The interaction corresponds to the regime where tip-sample separation is very small and tip experiences strong repulsive Coulombic interaction . Here deflection of the cantilever serves as a feedback parameter which is related to how hard the tip pushes against the surface. Deflection feedback is used to image a step topography. When the tip is over the flat area, feedback maintains the deflection at the setpoint. As the tip approaches the step, cantilever bends increasing the deflection above the setpoint. This change in deflection is seen as an error by the controller which gives a control signal that moves the z piezo away from the surface to revert the deflection back to the setpoint. As the surface drops away, deflection once again moves away from the setpoint in opposite direction. Once again, control loop responds to minimize this by giving a control signal that moves the z piezo towards the surface and deflection once again reverts to its nominal value. In this way, control signal itself becomes a representation of the surface.

Chapter 3

Local Ferroelectricity in Ge doped SnTe

3.1 Introduction

Heat is almost always encountered as a major waste by-product in the use of any form of energy. Thermoelectricity offers a mechanism of recovery of electricity from waste heat and is therefore a pivotal part of addressing the global energy management. Good thermoelectric performance of material require it to have low thermal conductivity. Materials with low thermal conductivity are rare to find but can be engineered via various techniques. Tellurides are supposed to show good thermoelectric performance and are used in power reactors[18]. Tin Telluride, which belongs to the same class was found to be a good thermal conductor and had ferroelectric ordering [19][20]. Recently, it was reported that SnTe could be engineered to show low thermal conductivity by doping it with Germanium[21]. This induces structural distortions in crytal and instable ferroelectric phase is observed. Absence of global ferroelectric ordering was reported here. In this chapter, I will be discussing local ferroelectricity does exist in Ge doped SnTe.

Here, we use temperature dependent piezoresponse force microscopy to directly show local polarization switching in $Sn_{1-x}Ge_xTe$, indicating ferroelectric behaviour, although global ferroelectric ordering has not been observed. We also observe clear

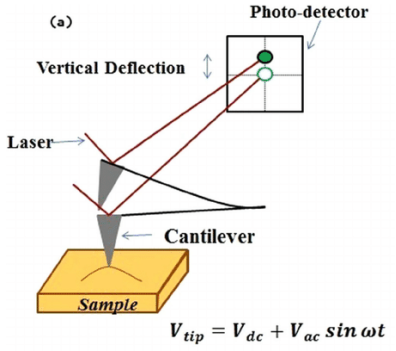

FIGURE 3.1: Schematic of PFM set up

Appl. Phys. Lett. 104, 162908 (2014); https://doi.org/10.1063/1.4873386

butterfly loops in local strain vs DC voltage which is a telltale sign of ferroelectricity. These measurements are carried out around the critical temperature of this material, reported to be 290K [21]. The observed ferroelectric behaviour supports the previous observation of low thermal conductivity in this material by engineering the ferroelectric instability.

3.2 PFM set up

In PFM setup, as shown in fig 3, we have a conductive cantilever in contact with the sample. A laser is directed on the cantilever and is reflected back to a quadrapole photo diode. A sinusoidal AC voltage V_{ac} is applied to the cantilever piezo chip connected to the cantilever. This drives the cantilever oscillation and the amplitude of the oscillation is measured as a function of frequency ω. This is done in order to find the resonant frequency of the cantilever in contact with the sample. All the measurements are then carried out at resonant frequency in order to achieve maximum sensitivity. In contact mode, the deflection of the cantilever is tracked while scanning it over a surface. PFM measures the mechanical response to the electrical field supplied between the tip and sample. The sample deforms i.e. locally expands or contracts in response to applied voltage, which in turn changes the deflection of cantilever. This deflection is interpreted in terms of response signal.

3.2.1 DART PFM

In contact mode, the tip is always in contact with sample. While scanning, the contact between the tip and sample change and so is the resonant frequency. This would increase the topographic crosstalk. To improve this situation, we use a technique called "Dual AC Resonance tracking" or DART PFM. In this mode, we use two lock in amplifiers to supply voltage to cantilever at two different frequencies. The oscillating voltage supplied is combination of two different frequencies ; one below the resonant frequency and one above it. The resultant deflection of the cantilever is sent back to lock in amplifiers which studies the amplitude change. The change in amplitude at these two frequencies is measured and the contact frequency is tracked by using the difference in amplitude of deflection at the two frequencies as feedback.

3.3 PFM Spectroscopy

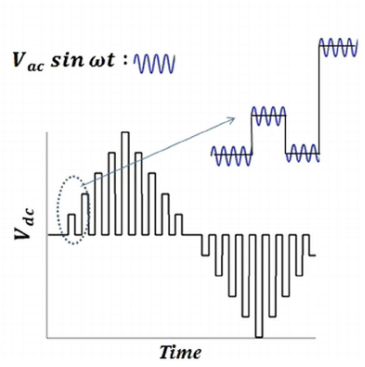

FIGURE 3.2: Combination of AC and DC signal in triangular saw tooth form for PFM spectroscopy

For PFM spectroscopy, a combination of AC voltage and DC voltage of the form $V_{tip} = V_{dc} + V_{ac}\cos(\omega t)$ is applied to the tip. A piezoelectric sample deforms below the tip in presence of applied voltage. The response signal is interpreted in terms of phase, the first harmonic component of the tip deflection. If the polarization direction below the tip is in direction with applied DC voltage, the sample would locally expand. So, a sweeping DC voltage would show a switching behaviour in phase. This can be observed as hysteric phase switching in ϕ vs V_{dc} curve.[22] The amplitude of

deformation can also be interpreted in a periodic form $A = A_0 + A_\omega cos(\omega t + \phi)$. This is observed as butterfly loop in A_ω vs V_{dc} curve. It should be noted that the hysteretic behaviour can be observed for reasons other can piezoelectricity such as electrostatic and electrochemical effects.

In order to mitigate the electrostatic effects, we supply a sequence of DC voltages with AC modulation in triangular saw tooth form as shown in fig. This switching spectroscopy protocol pioneered by Jesse *et al* allows us to measure the response signal in off state of pulses. The growth of nanoscale topographic features indicate electrochemical reaction over the surface.[23]

3.4 Results

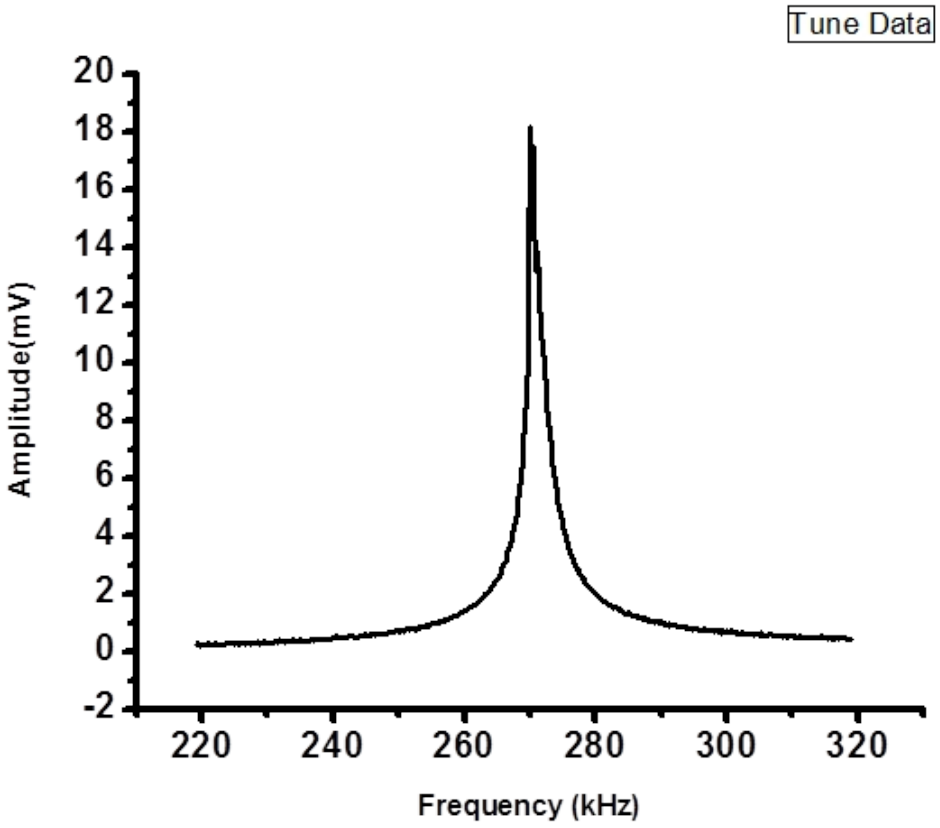

FIGURE 3.3: Frequency vs oscillation amplitude showing the resonant frequency

For PFM spectroscopic measurements, we took a 4mm x 4mm x 1mm SnGeTe sample and placed it over a metallic plate connected to a heating element. This plate, in turn, is grounded to high voltage amplifier. The temperature of the metallic plate can be varied from 278K to 400K. A conductive AFM tip, made of silicon coated with Platinum, was brought in contact with the sample. The free air resonant frequency was found to be around 73 kHz. The resonant frequency in contact with the sample was found to vary between 260 - 300 kHz. The spring constant of the cantilever was found to be 2.1 N/m.

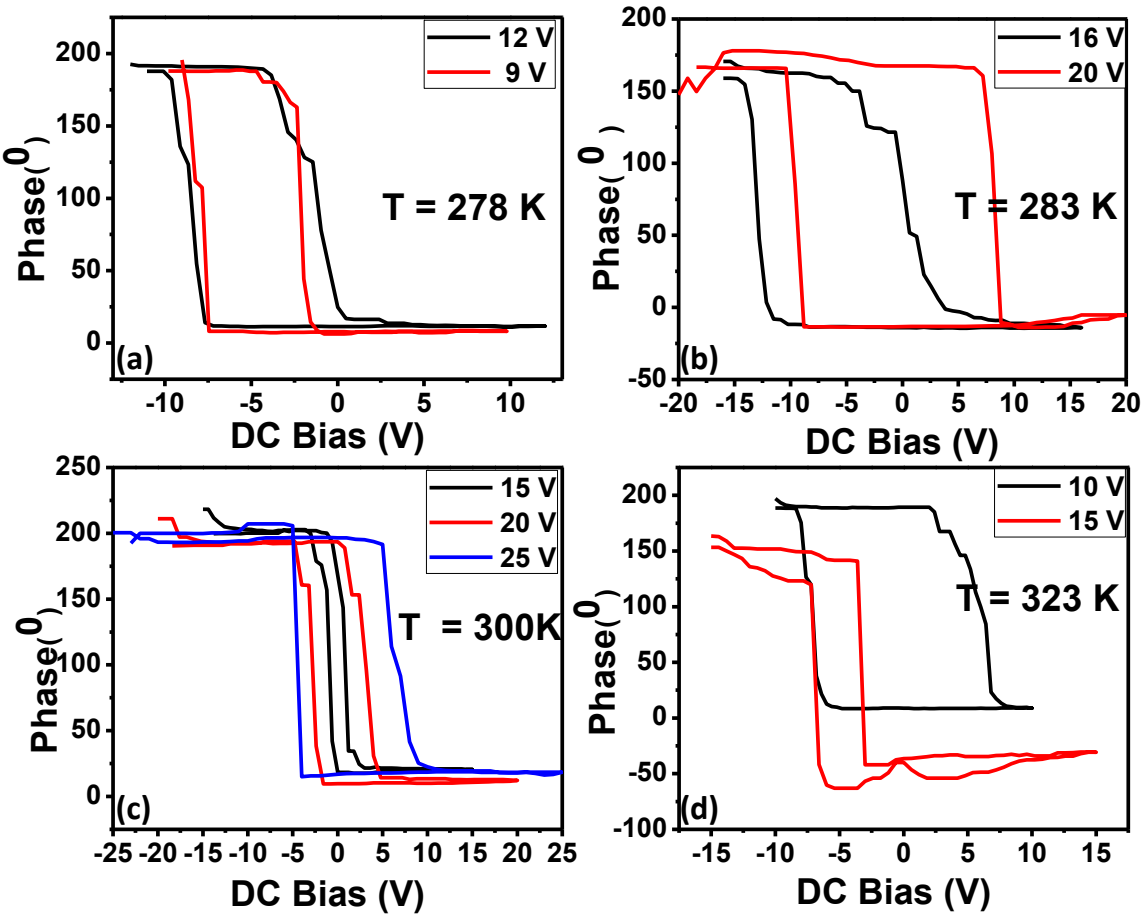

FIGURE 3.4: Phase vs V_{dc} switching curve at temperature (a) 278K (b) 283K (c) 300K and (d) 323K

Figures below show temperature dependence of the phase vs V_{dc} curve. Fig 3.4 clearly show hysteretic 180^0 phase switching at 278 K temperature with a fixed coercive voltage of 6V . The ferroelectric behaviour is confirmed by observing the same coercive voltage at different values of applied voltage. The plot betweeen Amplitude A_ω and

V_{dc} also show clear butterfly loop feature which further confirms ferroelectric behaviour. This measurement is carried out at sample temperatures 278 K, 283 K, 300 K and 323 K. The results are shown in fig . It can be seen that that the 180_0 phase switching is observed at all these temperatures but the coercive voltage does not remain fixed with applied maximum DC bias. The coercive voltage does not remain fixed at temperatures 300 K and 323 K. This is in accordance with the previously reported ferroelectric $T_c = 290K$

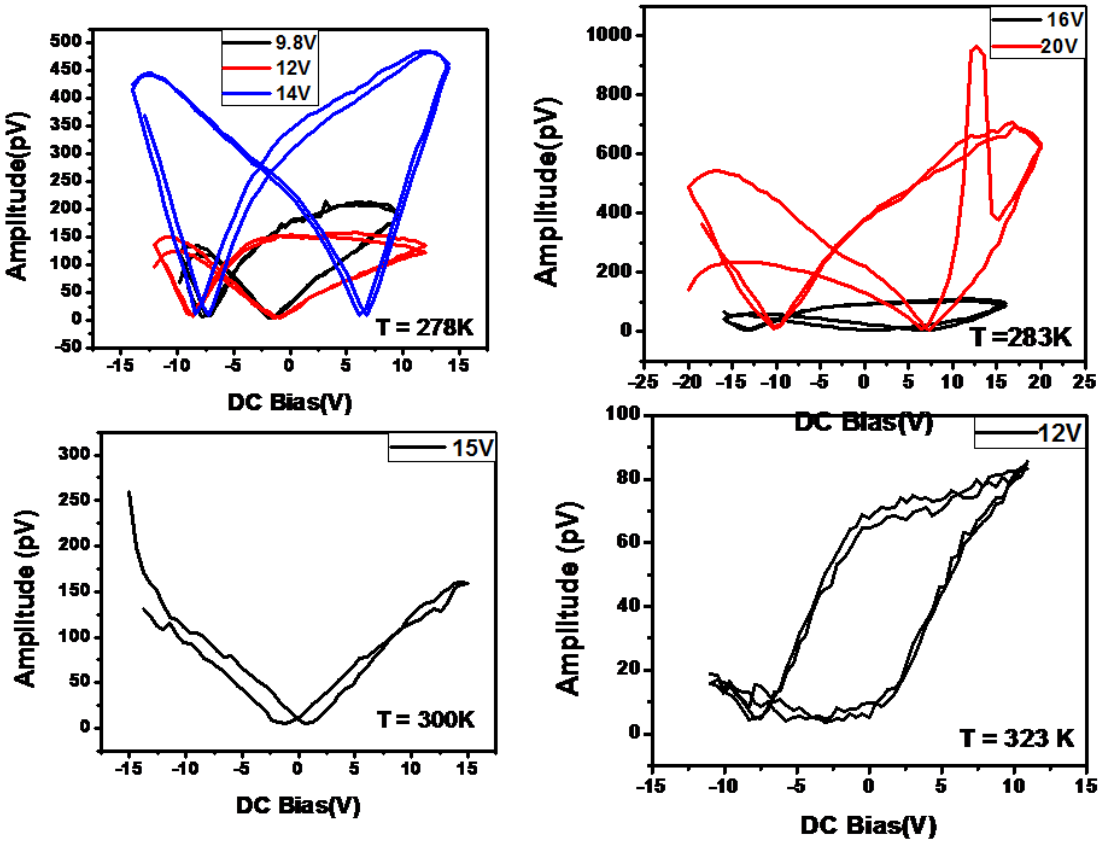

FIGURE 3.5: Temperature dependence of amplitude vs DC Bias (Butterfly loop)

For PFM imaging, we bring the tip in contact with the sample. An AC voltage V_{ac} is applied to the tip which moves over the sample in raster method using XY scanner attached to the stage. Meanwhile, the deflection of the cantilever is tracked. This is done via a feedback loop which maintains the deflection signal at a particular value. The error in deflection signal gives us information about the phase and amplitude of the response signal. If the electric polarization is opposite in two different domains, the measured value of ϕ varies by 180 between the two domains. By plotting the

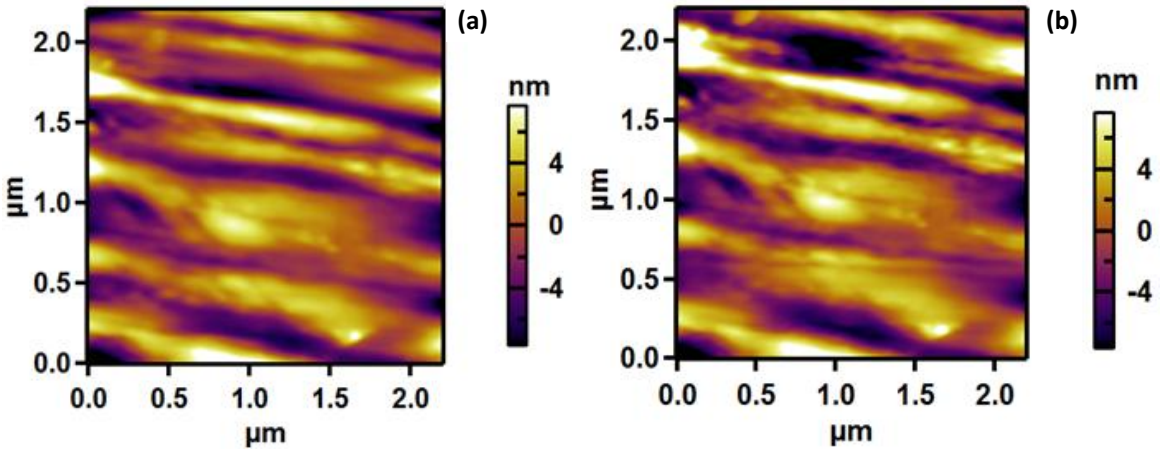

FIGURE 3.6: Topographic image before and after PFM spectroscopy

magnitude of ϕ as a function of the position of the tip, a PFM image exhibiting the distribution of ferroelectric domains on the sample surface is constructed. During PFM imaging, the resonance frequency might shift as the cantilever rubs against the surface and interacts differently with the sample at different points. In order to track the contact-resonance in real time, the measurements were done in so-called DART (dual ac resonance tracking) mode. In this mode, the contact resonance peak is tracked between two limit frequencies and the AC bias is then changed to maintain the peak at a particular value.

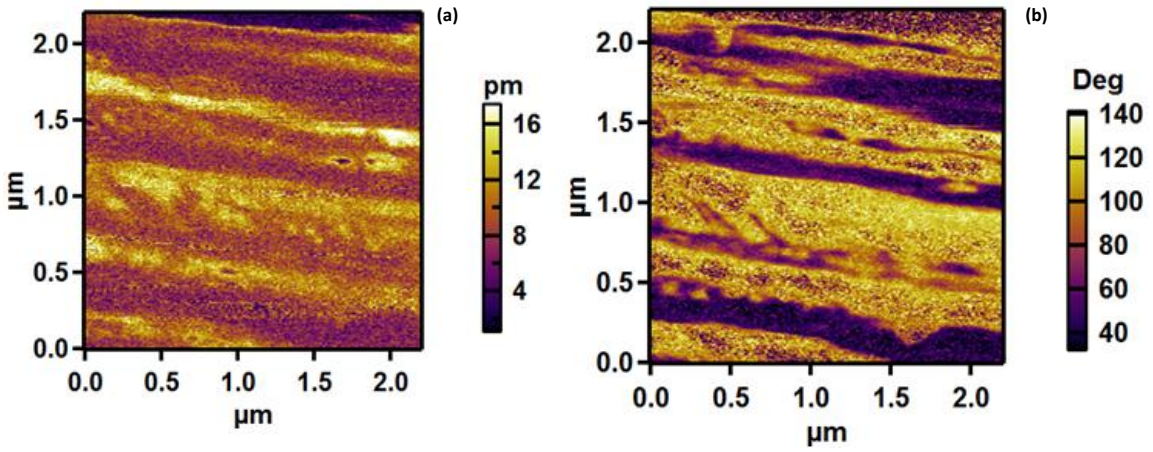

FIGURE 3.7: Amplitude and phase images resembling the topographic image

Figures below show the topographic image taken before and after doing PFM spectroscopy. It can be seen that the topography is very rough in both the images.

3.5 Conclusion

$Sn_{1-x}Ge_xTe$ was reported to show ferroelectric instability but we can clearly see polarization switching in sample at temperatures below critical temperature. So, although there is no global ferroelectric ordering in sample, local ferroelectricity does exist in material. The observed polarization switching above critical temperature can be attributed to electrochemical reaction between tip and sample. Since, the surface is very rough, we can not image the growth of nanostructure in areas of PFM spectroscopy. Clear butterfly loops are observed in amp vs applied DC voltage which is hallmark of ferroelectricity. We could not image the ferroelectric domains in the material due to high carrier density in crystal.

Thus, it can be concluded that local ferroelectricity can exist in absence of global ferroelectric ordering. The low thermal conductivity observed in SnGeTe coexists with local ferroelectricity.

Bibliography

[1] Yoichi Ando. Topological insulator materials. *Journal of the Physical Society of Japan*, 82(10):102001, 2013.

[2] Joel E Moore. The birth of topological insulators. *Nature*, 464(7286):194, 2010.

[3] Klaus Von Klitzing. The quantized hall effect. *Reviews of Modern Physics*, 58 (3):519, 1986.

[4] Marvin E Cage, Kv Klitzing, AM Chang, F Duncan, M Haldane, RB Laughlin, AMM Pruisken, and DJ Thouless. *The quantum Hall effect*. Springer Science & Business Media, 2012.

[5] Charles L Kane and Eugene J Mele. Z 2 topological order and the quantum spin hall effect. *Physical review letters*, 95(14):146802, 2005.

[6] Charles L Kane and Eugene J Mele. Quantum spin hall effect in graphene. *Physical review letters*, 95(22):226801, 2005.

[7] Markus König, Steffen Wiedmann, Christoph Brüne, Andreas Roth, Hartmut Buhmann, Laurens W Molenkamp, Xiao-Liang Qi, and Shou-Cheng Zhang. Quantum spin hall insulator state in hgte quantum wells. *Science*, 318(5851): 766–770, 2007.

[8] M Zahid Hasan and Charles L Kane. Colloquium: topological insulators. *Reviews of modern physics*, 82(4):3045, 2010.

[9] YL Chen, James G Analytis, J-H Chu, ZK Liu, S-K Mo, Xiao-Liang Qi, HJ Zhang, DH Lu, Xi Dai, Zhong Fang, et al. Experimental realization of a three-dimensional topological insulator, bi2te3. *science*, 325(5937):178–181, 2009.

[10] Yuqi Xia, Dong Qian, David Hsieh, L Wray, Arijeet Pal, Hsin Lin, Arun Bansil, DHYS Grauer, Yew San Hor, Robert Joseph Cava, et al. Observation of a large-gap topological-insulator class with a single dirac cone on the surface. *Nature physics*, 5(6):398, 2009.

[11] Bin Xia, Peng Ren, Azat Sulaev, Peng Liu, Shun-Qing Shen, and Lan Wang. Indications of surface-dominated transport in single crystalline nanoflake devices of topological insulator bi 1.5 sb 0.5 te 1.8 se 1.2. *Physical Review B*, 87(8): 085442, 2013.

[12] T Arakane, T Sato, S Souma, K Kosaka, K Nakayama, M Komatsu, T Takahashi, Zhi Ren, Kouji Segawa, and Yoichi Ando. Tunable dirac cone in the topological insulator bi 2-x sb x te 3-y se y. *Nature communications*, 3:636, 2012.

[13] KS Novoselov, D Jiang, F Schedin, TJ Booth, VV Khotkevich, SV Morozov, and AK Geim. Two-dimensional atomic crystals. *Proceedings of the National Academy of Sciences*, 102(30):10451–10453, 2005.

[14] https://www.azonano.com/article.aspx?articleid=2682.

[15] Asylum research manuals for mfp-3d.

[16] G Binning and CF Quate. Gerber ch 1986 atomic force microscope. *Phys. Rev. Lett*, 56(9):930.

[17] Franz J. Giessibl. Advances in atomic force microscopy. *Rev. Mod. Phys.*, 75: 949–983, Jul 2003. doi: 10.1103/RevModPhys.75.949. URL https://link.aps.org/doi/10.1103/RevModPhys.75.949.

[18] Li-Dong Zhao, Shih-Han Lo, Yongsheng Zhang, Hui Sun, Gangjian Tan, Ctirad Uher, Christopher Wolverton, Vinayak P Dravid, and Mercouri G Kanatzidis. Ultralow thermal conductivity and high thermoelectric figure of merit in snse crystals. *Nature*, 508(7496):373, 2014.

[19] Joseph P Heremans, Vladimir Jovovic, Eric S Toberer, Ali Saramat, Ken Kurosaki, Anek Charoenphakdee, Shinsuke Yamanaka, and G Jeffrey Snyder. Enhancement of thermoelectric efficiency in pbte by distortion of the electronic density of states. *Science*, 321(5888):554–557, 2008.

[20] Leena Aggarwal, Ananya Banik, Shashwat Anand, Umesh V Waghmare, Kanishka Biswas, and Goutam Sheet. Local ferroelectricity in thermoelectric snte above room temperature driven by competing phonon instabilities and soft resonant bonding. *Journal of Materiomics*, 2(2):196–202, 2016.

[21] Ananya Banik, Tanmoy Ghosh, Raagya Arora, Moinak Dutta, Juhi Pandey, Somnath Acharya, Ajay Soni, Umesh V Waghmare, and Kanishka Biswas. Engineering ferroelectric instability to achieve ultralow thermal conductivity and high thermoelectric performance in sn 1- x ge x te. *Energy & Environmental Science*, 12(2):589–595, 2019.

[22] Brian J Rodriguez, Clint Callahan, Sergei V Kalinin, and Roger Proksch. Dual-frequency resonance-tracking atomic force microscopy. *Nanotechnology*, 18(47): 475504, 2007.

[23] Jagmeet S Sekhon, Leena Aggarwal, and Goutam Sheet. Voltage induced local hysteretic phase switching in silicon. *Applied Physics Letters*, 104(16):162908, 2014.